Topographical Organization of the N-Terminal Segment of Lung Pulmonary Surfactant Protein B (SP-B_{1-25}) in Phospholipid Bilayers

Yudong Wang,[‡,§,||] K. Murali K. Rao,[‡,||] and Eugene Demchuk*,[‡,§]

Health Effects Laboratory Division, National Institute for Occupational Safety and Health, Morgantown, West Virginia 26505, and Department of Biochemistry and Molecular Pharmacology, West Virginia University School of Medicine, Morgantown, West Virginia 26506, and School of Pharmacy, West Virginia University, Morgantown, West Virginia 26506

Received December 11, 2002; Revised Manuscript Received January 24, 2003

ABSTRACT: The location and depth of each residue of lung pulmonary surfactant protein B (SP-B_{1-25}) in a phospholipid bilayer (PB) was determined by fluorescence quenching using synthesized single-residue-substituted peptides that were reconstituted into 1,2-dipalmitoyl phosphatidylcholine (DPPC)-enriched liposomes. The single-residue substitutions in peptides were either aspartate or tryptophan. The aspartate was subsequently labeled with the *N*-cyclohexyl-*N*′-(4-(dimethylamino)naphthyl)carbodiimide (NCD-4) fluorophore, whereas tryptophan is autofluorescent. Spin-labeled compounds, 5-doxylstearic acid (5-DSA), 7-doxylstearic acid (7-DSA), 12-doxylstearic acid (12-DSA), 4-(*N*,*N*-dimethyl-*N*-hexadecyl)ammonium-2,2,6,6-tetramethylpiperidine-1-oxyl iodide (CAT-16), and 4-trimethylammonium-2,2,6,6-tetramethylpiperidine-1-oxy iodide (CAT-1), were used in the quenching experiments. The effective quenching order is determined by the accessibility of the quencher to a fluorescent group on the peptide. The order of quenching efficiency provides information about the relative locations of individual residues in the PB. Our data indicate that residues Phe1−Pro6 are located at the surface of PB, residues Tyr7−Trp9 are embedded in PB, and residues Leu10−Ile22 are involved in an amphipathic α-helix with its axis parallel to the surface of PB; residues Pro23−Gly25 reside at the surface. The effects of intermolecular disulfide bond formation in the SP-B_{1-25} dimer were also investigated. The experiments suggest that the SP-B helix A has to rotate at an angle to form a disulfide bond with the neighboring cysteine, which makes the hydrophobic sides of the amphipathic helices face each other, thus forming a hydrophobic domain. The detailed topographical mapping of SP-B_{1-25} and its dimer in PB provides new insights into the conformational organization of the lung pulmonary surfactant proteins in the environment that mimics the native state. The environment-specific conformational flexibility of the hydrophobic domain created by SP-B folding may explain the key functional properties of SP-B including their impact on phospholipid transport between the lipid phases and in modulating the cell inflammatory response during respiratory distress syndrome.

Pulmonary surfactant is a product secreted by the lung epithelial type II pneumocytes. A major function of the surfactant is to reduce the surface tension across the air/liquid interface, thereby preventing alveolar collapse (or atelectasis) during lung deflation (*1*). The surfactant material has the unique ability to coherently adjust the thickness and tension of surface lining film during the ventilation cycle in response to the changing volume of alveoli.

Lung surfactant consists of approximately 90% lipid and 10% protein by mass (*2*). The lipid component, compositionally, is a mixture of 1,2-dipalmitoyl phosphatidylcholine (DPPC)[1] and minor fractions of acidic, unsaturated, and neutral lipids. Taken alone, the lipid component is at least an order of magnitude less efficient in adsorbing to the air/liquid interface than the whole surfactant (*3*, *4*). The difference in efficiency is attributed to a comparatively small but crucially important protein component of the surfactant. There are at least four surfactant apoproteins, designated as the surfactant protein A (SP-A), SP-B, SP-C and SP-D (*5*). SP-A and SP-D are relatively large collagenous carbohydrate-binding hydrophilic glycoproteins. SP-B and SP-C are smaller surfactant-associated hydrophobic proteins. They are directly interspersed into the lipid component of surfactant, generating and maintaining the surface-active monolayer film. SP-B has been ascribed many essential physiological functions. These include promotion of lipid adsorption to the air/liquid interface, dynamic surface tension lowering and improvement of pressure−volume mechanics (*3*, *6*, *7*),

* To whom correspondence should be addressed. Address: HELD/NIOSH, 1095 Willowdale Road, Morgantown, WV 26505-2888. Telephone: (304) 285-6034. Fax: (304) 285-6041. E-mail address: EDemchuk@cdc.gov.

[‡] National Institute for Occupational Safety and Health.

[§] West Virginia University.

[||] Author E-mail addresses: YWang2@cdc.gov, MRao@cdc.gov.

[1] Abbreviations: SP-B, surfactant protein B; PB, phospholipid bilayer; Chl, chloroform; MeOH, methanol; DPPC, dipalmitoyl phosphatidylcholine; PC, phosphatidylcholine; PG, L-phosphatidyl-DL-glycerol; CAT-16, 4-(*N*,*N*-dimethyl-*N*-hexadecyl)ammonium-2,2,6,6-tetramethylpiperidine-1-oxyl iodide NCD-4, *N*-cyclohexyl-*N*′-(4-(dimethylamino)naphthyl)carbodiimide; CAT-1, 4-trimethylammonium-2,2,6,6-tetramethylpiperidine-1-oxy iodide 5-DSA, 5-doxylstearic acid; 7-DSA, 7-doxylstearic acid; 12-DSA, 12-doxylstearic acid; CD, circular dichroism; NMR, nuclear magnetic resonance; DTT, dithiothreitol; FTIR, Fourier-transform infrared spectroscopy; RP-HPLC, reversed-phase high-performance liquid chromatography.

10.1021/bi027344h
Published on Web 03/21/2003

thermodynamics of surfactant adsorption and respreading of films from the collapse phase (*8*, *9*), stabilization of lipid monolayer films, membrane binding, and membrane fusion (*10*, *11*), and antimicrobial activity (*12*, *13*). Deficiency of SP-B results in disruption of lamellar bodies and tubular myelin formation, loss of type II pneumocyte polarity (*14*), and massive discharge of disrupted lamellar bodies into the airway (*15*).

SP-B is a 79-amino acid residue lipophilic apoprotein. It contains 52% hydrophobic amino acids and a substantial number of basic groups, resulting in the net charge of +7. SP-B is found as a ~17 kDa sulfhydryl-dependent homodimer (*16*). The monomer is presumed to consist of four (*17*) or five (*18*) amphipathic helices bundled together by intramolecular disulfide bridges. The bridges are formed between highly conserved cysteine residues. They are Cys8−Cys77, Cys11−Cys71, and Cys35−Cys46 (*17*). The remaining Cys48 forms an intermolecular disulfide bond responsible for dimerization. The pattern of intramolecular disulphide bonds and overall sequence similarity to sphingolipid-activator proteins (saposins) establish SP-B as a representative of the saposin-like protein family (*19*). However, unlike other members of this family, SP-B is more lipophilic, is permanently lipid-associated, and exists as a dimer. At least one three-dimensional structural model of SP-B has been reported. It is for porcine SP-B on the basis of its 22% sequence identity to NK-lysin, the only saposin-like domain for which coordinates have been determined experimentally (*20*). Despite the marginal sequence homology, the model successfully confirmed the approximate locations of all four major α-helices. In addition, it predicted a new previously unknown α-helix presumably adjacent to the helix D. Yet, the proposed spatial arrangement of the helices in the lipid-associated mode needs additional corroboration; because NK-lysin is water-soluble but SP-B is not, the model carries no information about the tertiary structure of SP-B in ordered lipid films.

Because of a specific mode of SP-B−lipid association, in which extreme hydrophobicity of the protein coexists with a substantial cationic charge, structural studies of SP-B in the native phospholipid environment have proven to be technically challenging. Therefore, it was concluded that SP-B association with phospholipids may represent a more complex mode than that of other membrane-spanning species (*21*). The topographical organization of SP-B with respect to the phospholipid environment was mainly studied using synthetic analogues of the protein. Previous findings revealed that in many instances a short positively charged N-terminal fragment, which contains only the first 25 amino acids (SP-B_{1-25}), can effectively replace the full-length SP-B. For instance, (1) in model surfactant films, both increase the collapse pressure (while uncharged mutants do not), suggesting that the cationic N-terminus of SP-B interacts with anionic lipids to remove the driving force for lipid collapse from the surface film (*22*−*25*); (2) according to pressure−area isotherms, Brewster angle microscopy, and grazing incidence X-ray diffraction measurements in mixtures, both increase the fraction of fluid phase in the liquid-expanded/liquid-condensed two-phase region (*26*); (3) both, and especially a dimeric form of SP-B_{1-25}, efficiently reduce the surface tension in surface films (*27*); (4) both improve in vivo function and sensitivity to plasma inhibition of clinical surfactant in premature neonates (*28*, *29*). These observations underscore the critical importance of SP-B_{1-25} to the native function of full-length SP-B. Therefore, elucidation of the topographical organization of SP-B_{1-25} in the PB environment may be helpful in understanding the structure and function of SP-B.

Interactions of SP-B and its fragments in lipid bilayers and monolayers have been investigated using various experimental and theoretical techniques, such as attenuated total reflection Fourier-transform infrared (FTIR) spectroscopy (*30*), external reflection−absorption infrared spectroscopy (*31*, *32*), ^{13}C-FTIR (*33*, *34*), circular dichroism (CD) (*32*−*37*), nuclear magnetic resonance (NMR) (*38*−*41*), Raman spectroscopy (*42*), fluorescence anisotropy (*43*), tryptophan fluorescence (*40*), and molecular modeling and molecular dynamics simulations (*20*, *44*). Most studies support a model in which the amphipathic helices of SP-B interact with the polar headgroup region of PB with its helical axes oriented roughly parallel to the surface of the lipid−water interface (*43*), the polar faces of the amphipathic helices interact with solvent and phospholipid headgroups; the positively charged residues interact electrostatically with anionic phospholipid components of the surfactant, and the hydrophobic regions face the acyl chains of phospholipids (*21*, *30*, *37*). On the other hand, some observations suggest that SP-B_{1-25} may be oriented at an oblique angle to the surface and partially embedded in the lipid films (*44*). In addition, there are differences in the literature concerning the length of the helix portion of SP-B_{1-25} and the location of Trp9 on PB. Further work is needed to answer these and other questions concerning the structural mode of SP-B when it is anchored to phospholipids in the water−lipid environment.

Fluorescence-quenching experiments that we performed provide information about the location and depth of each of the 25 SP-B_{1-25} residues in PB. The method involves synthetic single-residue-substituted peptides, which allow attachment of only one specific fluorescent group per peptide. These peptides are used for measurement of the relative efficiencies of quenching of peptide fluorescence by a spin-labeled probe either attached at a certain position on the lipid or dissolved in the aqueous phase (*45*−*47*). Comparative analysis of relative quenching efficiencies with respect to a specific spin-probe gives information on whether the fluorescent group interacts with the probe. Only the groups within a short contact distance interact. The quenching group can be attached to the lipid at different locations on the fatty acid. For instance, in our experiments, lipids with fatty acids labeled at positions of carbon-5, carbon-7, carbon-12, and the phosphate group were used. The location of a fluorophore-labeled residue with respect to PB is determined by the relative order of the measured quenching efficiencies.

Based on the sequence of human SP-B, the SP-B_{1-25}-mimic peptides, which carried either tryptophan or aspartate single-residue substitutions at each amino acid position, were synthesized and tested. Our studies suggest a topographical model of SP-B_{1-25} in which the N-terminal residues Phe1−Pro6 are located at the surface of PB, residues Tyr7−Trp9 are embedded in PB, residues Leu10−Ile22 (or Cys8−Ile22) form an amphipathic helix with its axis roughly parallel to the surface of BP, and residues Pro23−Gly25 are found at the surface of PB, similar to Phe1−Pro6.

Table 1: Amino Acid Sequences of Synthesized Peptides Represented by One-Letter Codes

	human[a] SP-B_{1-25}	F	P	I	P	L	P	Y	C	W	L	C	R	A	L	I	K	R	I	Q	A	M	I	P	K	G
1	P6D						D																			
2	Y7D							D																		
3	C8D								D																	
4	W9D									D																
5	L10D										D															
6	C11D											D														
7	R12D												D													
8	A13D													D												
9	L14D														D											
10	I15D															D										
11	K16D																D									
12	R17D																	D								
13	I18D																		D							
14	F1W/Q19D[b]	W								Y										D						
15	P2W/A20D[b]		W							Y											D					
16	I3W/M21D[b]			W						Y												D				
17	P4W/I22D[b]				W					Y													D			
18	L5W/P23D[b]					W				Y														D		
19	P6W/K24D[b]						W			Y															D	
20	P2W·P4A·P6A/G25D[b]		W		A		A			Y																D

[a] Only substitutions are shown. The rest of the sequence remains intact. [b] A "silent" W9Y substitution is not included in the peptide name.

MATERIALS AND METHODS

Materials. Chloroform (Chl), methanol (MeOH), 1,2-dipalmitoyl phosphatidylcholine (DPPC), phosphatidylcholine (PC), L-phosphatidyl-DL-glycerol (PG), and cholesterol were purchased from Sigma (St. Louis, MO). *N*-Cyclohexyl-*N*′-(4-(dimethylamino)naphthyl)carbodiimide (NCD-4) and spin-labeled probes, 4-trimethylammonium-2,2,6,6-tetramethylpiperidine-1-oxy iodide (CAT-1), 4-(*N*,*N*-dimethyl-*N*-hexadecyl)ammonium-2,2,6,6-tetramethylpiperidine-1-oxyl iodide (CAT-6), 5-doxylstearic acid (5-DSA), 7-doxylstearic acid (7-DSA), and 12-doxylstearic acid (12-DSA), were obtained from Molecular Probes, Inc. (Eugene, OR).

Peptide Design. Twenty peptides of the first 25 residues of SP-B deduced from the sequence of human SP-B were synthesized. An aspartate substitution was introduced into each peptide, replacing one residue at a time. To test two residues by using a single peptide, tryptophan was also introduced in several triple-substituted peptides and in one penta-substituted peptide. To keep only one tryptophan residue per peptide, each multiple-substituted peptide carried a silencing W9Y substitution, along with two or more test mutations. These included F1W/Q19D, P2W/A20D, I3W/M21D, P4W/I22D, L5W/P23D, P6W/K24D, and P2W·P4A·P6A/G25D peptides. The substituted peptides probed in this study are shown in Table 1.

Peptide Synthesis. The Peptide Synthesis Facility of the Molecular Medicine Institute at the Center for Biotechnology and Bioengineering of the University of Pittsburgh synthesized the peptides. The peptides were synthesized on an Omega 396 automated peptide synthesizer (Advanced ChemTech, Louisville, Kentucky) following the FMOC synthesis protocol. Crude peptides were analyzed, characterized, and purified by gel filtration (G-25 column), reversed-phase high performance liquid chromatography (RP-HPLC, 486 and 600E by Waters Corporation). The correct mass was later confirmed by electrospray mass spectroscopy (Quattro II, Fisons Inc.).

Labeling of Synthesized Peptides with NCD-4 and Incorporation into Proteoliposomes. The synthesized peptides were suspended in methanol and incubated with NCD-4 in a molecular ratio of 40 nM NCD-4 to 1 nmol of peptide for 1 h at room temperature. The unbound reagent was removed by dialysis with three separate changes of methanol. To prevent peptide aggregation, 1:2 (peptide/lipid, g/g) of lipid in a mixture, as described below, was added into the suspension before the mixture was dried under a continuous stream of nitrogen gas. The lipid/labeled peptide complex was suspended in a buffer containing 100 mM KCl, 200 mM sucrose, and 30 mM Tris-HCl, pH 7.0, at a final protein concentration of 8 mg/mL.

Proteoliposomes were prepared as described previously (*27*, *47*) but with some modifications. Fifty milligrams of the lipid mixture DPPC/PG/PC/cholesterol (25:12.5:5:7.5) was suspended in a solvent of Chl/MeOH (1:2, v/v). The lipid solution was dried under a continuous stream of nitrogen at room temperature and resuspended in the buffer described above to a final concentration of 50 mg/mL of lipid. The suspension was vortexed and incubated at 55 °C for 15 min. The liposomes thus formed were sonicated for 1 min 2 times at 37 °C with a 30-s interval. NCD-4 (or tryptophan)-labeled peptide was added to the liposome suspension at a ratio 1:50 (peptide/lipid) and incubated for 1 h at 37 °C. Because of the partial overlap between tryptophan emission and NCD-4-labeled aspartate absorption bands, only a single fluorophore group per each quenching experiment was used, that is, multiple-substituted peptides were not labeled with NCD-4 in quenching experiments in which tryptophan was used as a source of autofluorescence. The peptides were labeled with NCD-4 only when an aspartate substitution was used as a probe. To minimize possible interactions between fluorophores in multiple-substituted peptides, the tryptophan and aspartate substitutions were introduced at a distance of at least 18 residues from each other.

Fluorescence Quenching Experiments. A single tryptophan substitution provides a position-related autofluorescent label. Its excitation occurs at the wavelength of 275−295 nm and its emission at 340 nm (*48*). NCD-4 has been reported to bind to carboxyl groups of acidic amino acids on proteins and produce fluorescence (*49*). Its emission maximum is at 425 nm in 100% ethanol and 440 nm in 50% ethanol. The

emission spectrum observed after the reaction of NCD-4 with acidic amino acids is consistent with the formation of an *N*-acetyl urea formed by carboxyl-coupled NCD-4. Thus, a single-aspartate-substituted peptide, followed by labeling with NCD-4, also provides a position-dependent fluorescent label with its excitation and emission maxima at 334 and 422 nm, respectively.

To obtain information on localization of the fluorescent probe with respect to the surface of PB, a series of paramagnetic fluorescence-quenching experiments (*17*, *46*, *50*) were carried out. The group of spin-labeled compounds applied in this study includes 5-DSA, 7-DSA, and 12-DSA, which are the derivatives of stearic acid with a nitroxide radical ring substitution introduced, respectively, at the 5th, 7th and 12th carbon atom positions on the acyl chain, CAT-16, a cationic amphiphilic spin label with a polar group—its spin label is located at the PB surface, and a water-soluble CAT-1, which was the most polar spin label used in the experiments. Dynamic collisional quenching obeys the Stern−Volmer relationship (*49*):

$$I_0/I = 1 + K_D[Q] \quad (1)$$

where I_0 and I are the fluorescence intensities in the absence and presence of the quencher, [Q] is the concentration of the quencher, and K_D is the Stern−Volmer quenching constant. The Stern−Volmer relationship was analyzed by plotting the observed order of quenching efficiency ($I_0/I - 1$) against [Q].

The fluorescence intensities were determined using a dual-scanning luminescence spectrometer from Perkin-Elmer (Norwalk, CT, model LS-50B). Measurements were performed at 37 °C. Fluorescence quenching was performed in 2 mL of reaction buffer containing 100 mM KCl, 200 mM sucrose, and 30 mM Tris-HCl, pH 7.0. The quenchers CAT-16, 5-DSA, 7-DSA, and 12-DSA were prepared at 20 mM stock solution in ethanol and were added to the reaction mixtures at final concentrations of 10, 25, 50, 75, and 100 μM. CAT-1 was prepared at 100 or 200 mM stock solution and was added to the reaction mixtures at final concentrations of 1, 1.5, 2, and 2.5 mM.

Formation of Dimer Peptide. A C8D mutation peptide was used. It forms a dimer under conditions described previously (*27*). In this peptide, Cys11 is the only cysteine that is able to participate in the formation of an intermolecular disulfide bond between the monomeric peptides. The peptide was reduced with 100 mM dithiothreitol (DTT) for 12 h in a solution containing 30 mM Tris-HCl and 100 mM KCl, pH 7.5, with 50% methanol at a concentration of 1 mg/mL protein. The peptide suspension was then dialyzed three times with a buffer (30 mM Tris-HCl, 100 mM KCl, pH 7.5, with 50% methanol) to remove the unreacted DTT. The peptide suspension was stirred for 2 days under air-oxidation conditions. During this period, the dimers were formed. The formation of dC8D homodimers was confirmed by SDS−PAGE.

Molecular Modeling. A three-dimensional model of SP-B_{1-25} was rendered using CHARMM (*51*), Insight II, and Cerius^2 from Accelrys, Inc. (San Diego, CA). The initial setup of the peptide was carried out in internal coordinates as implemented in CHARMM. All ω-angles were assumed to have the trans conformation. On the basis of the results of fluorescence-quenching experiments, ϕ-angles of residues 11−22 and ψ-angles of residues 10−21 were assigned −65° and −40°, respectively.

As a test case, ten N-terminal residues were assumed in six standard canonical conformations as given by the Biopolymer module of Insight II. They are the right α-helix, left α-helix, 3_{10}-helix, π-helix, β-strand, and the extended conformation. When necessary, the N-terminal 10-mer of SP-B_{1-25} was then adjusted to match a hypothetical plane of the lipid−water interface. In all but one case, this was achieved by manual variation of the ϕ_{11} angle. However, in the extended conformation, in addition to that, the ψ_3 angle also had to be adjusted. Next, all test structures were subjected to 500 cycles of unrestrained adopted basis Newton−Raphson energy minimization in vacuum using the CHARMM27 all-atom force field (*52*) with dielectric constant of 1.0 and distant-dependent screening factor. Ionizable groups and the termini were assumed to have their standard protonation states at pH 7. All minimizations were carried out without truncation of nonbonded interactions.

Using these procedures, we identified the best-fitting standard conformation. It was the extended conformation. We further used this conformation as the starting point for refinement of the structural model. Residues 1−10 were assigned the extended conformation in Insight II and then manually modified to maximally account for the results of fluorescence-quenching experiments. After these manipulations, the model was minimized following the protocol explained above.

RESULTS

Quenching effects of spin labels on the fluorescence of NCD-4-labeled single-residue-substituted peptides and autofluorescence of single-tryptophan-substituted peptides were analyzed using eq 1. The most effective quenchers were CAT-1, CAT-16, and 5-DSA. 7-DSA showed a rather weak quenching efficiency comparing to these three quenchers. Overall, it suggests that SP-B_{1-25} does not penetrate deep inside PB, and that is consistent with the view that SP-B_{1-25} may be an amphipathic peptide that is located at the surface of PB. More careful analysis of the data suggests that some of the residues are associated with the polar environment, some are located at the surface of the lipid−water interface, and some are embedded somewhat deeper in PB. The deepest-embedded residue stretches into PB up to approximately the carbon-5 of the fatty acid chains. The weak quenching efficiency of 7-DSA and complete lack of 12-DSA quenching indicate that SP-B_{1-25} does not have a transmembrane domain.

The observed order of quenching efficiency can be divided into three groups (Table 2). The quenching profile of group I consists of a polar quencher, CAT-1, as the only effective quencher (Figure 1) and CAT-16 having a minor quenching efficiency, if any at all. The hydrophobic quenchers 5-DSA and 7-DSA had no effect on the fluorescence quenching whatsoever. This suggests that the residues in group I are located in the aqueous environment. Figure 1 shows the quenching profile of mutation peptide K16D, which is representative of the six peptides in group 1.

In group II, the amphiphilic probe CAT-16 and hydrophilic spin-labeled quencher CAT-1 were both effective quenchers.

Table 2: The Three Groups of Residues of SP-B_{1-25} Based on Their Relative Locations in the Lipid Bliayer as Determined by Fluorescence-Quenching Experiments[a]

		group III	
group I	group II	shallow	deeper
R12	F1	C8	Y7
A13	P2	L14	W9
R16	I3	M21	C11
R17	P4		I15
Q19	L5		I18
A20	P6		I22
	L10		
	O23		
	K24		
	G25		

[a] Group I residues are in the water environment; group II residues are located near the headgroups of phospholipids; group III amino acids are embedded in the lipids.

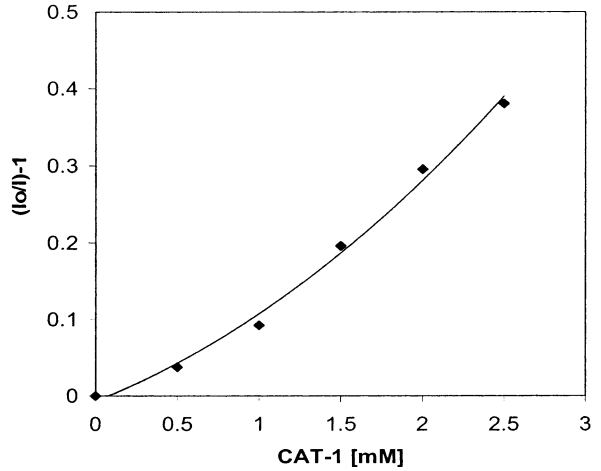

FIGURE 1: Fluorescence quenching of K16D, representing group I peptides. The peptides incorporated into liposomes were suspended in 2 mL of reaction buffer containing 40 μg/mL of the peptides. The reaction was performed at 37 °C. After 4 min of equilibration time, the fluorescence intensity was recorded as described in the Materials and Methods section. The plot was calculated using eq 1. Each point on the plot is the average of three or more experiments.

The hydrophobic quencher 5-DSA showed either weak or no quenching. 7-DSA has no quenching effect at all on peptides in this group. The order of quenching efficiency for this group was CAT-16 $\gg$ 5-DSA; and CAT-1 exhibited significant quenching efficiency at low concentrations (Figure 2). Therefore, the residues in this group appear to be located at the surface of PB in contact with the headgroups of phospholipids. At position six, the conclusion was supported by substitutions of two kinds. Both tryptophan (P6W) and aspartate (P6D) substitutions yielded very similar quenching properties. This suggests that there was no significant difference in the topography of the lipid-embedded peptide when either tryptophan or aspartate was used as a substituent in the synthesized peptides.

In group III, the hydrophobic quencher 5-DSA showed the most powerful quenching efficiency as compared to the amphiphilic quencher CAT-16 and deep lipid-embedded probe 7-DSA. The observed quenching order was either 5-DSA $\geq$ CAT-16, and CAT-1 shows effective quenching (Figure 3A1,A2) or 5-DSA > 7-DSA > CAT-16 with no appreciable quenching from the polar quencher CAT-1 (Figure 3B). Nine peptides belong to this group.

The quenching efficiency data for group III peptides indicate that the relevant residues are embedded in the lipid environment but not deep enough to reach 12-DSA or even 7-DSA. Some of them appear to be shallow, but some are embedded more deeply in PB. The nearly equal quenching efficiency by amphiphilic quencher CAT-16 and 5-DSA (5-DSA $\geq$ CAT-16) suggests that a residue is located between the surface of PB and carbon-5 of the fatty acid chain at approximately 1−2 Å from the surface of PB (Figure 3A1,-A2). Three peptides, C8D, L14D, and M21D, show that their fluorescent groups are shallowly embedded in PB. On the other hand, when the observed quenching efficiency order is 5-DSA > CAT-16 or 5-DSA > 7-DSA > CAT-16 and CAT-1 shows no quenching at all, the fluorescent groups of the peptides are embedded in PB close to carbon-5 of the fatty acid chain. There are six peptides satisfying these criteria; they are Y7D, W9D, C11D, I15D, I18D, and I22D (Figure 3B). In all these cases, 7-DSA showed very weak quenching efficiency and 12-DSA did not show quenching at all. This suggests that there is no residue of SP-B_{1-25} that is located deeper than or even reaches carbon-7 of the fatty acid chains. In fact, most of these residues are around carbon-5 of the fatty acid chains.

Table 3 summarizes the quenching data for all 25 residues of SP-B_{1-25} as they are found in the native sequence. The table also shows the location of each residue with respect to PB and a proposed molecular conformation of the residue. On the basis of these data, we propose the following topographical model of human SP-B_{1-25}. The first six residues, from Phe1 to Pro6, are located at the surface of PB. Residues Tyr7 to Trp9 are embedded in PB. Cys8 is also lipid-embedded but more shallowly than Tyr7 and Trp9. The quenching efficiency of peptides with substitutions from Leu10 to Ile22 showed a regular periodic shift of the residues between polar and nonpolar environments. There are about three to four residues per pitch (Table 2). The regularity of this pattern complies with the canonical definition of α-helix. Taking into account that both the C- and N-terminal residues are located at the surface and to satisfy conditions imposed by the measurements on Leu10- to Ile22-substituted peptides, the α-helix has to be located at the surface of PB with its axis approximately parallel to the lipid−water interface. Relative locations of each residue with respect to PB are shown in Figure 4. According to molecular modeling (see below), Leu10 appears to be the first residue involved in the hydrogen-bonding network of the helix. It is located at the surface of PB. Other helix residues cycle between the polar and nonpolar regions in agreement with the helical wheel diagram. Some residues of the helix, Arg12, Ala13, Lys16, Arg17, Gln19, and Ala20, are oriented toward the polar environment, while others, Ile15, Ile22, Cys11, Ile18, Leu14, and Met21, are located at the opposite side, which is embedded in PB. The side chains of Cys11 and Ile18 are the deepest and must be located at the bottom of the hydrophobic side of the amphipathic helix, probably about 3−6 Å deep from the PB surface. The relative arrangement of Arg12 and Gln19 deserves a separate comment. According to the Edmundson helical wheel, residue Gln19 should be somewhat closer to PB than Arg12. However, our data showed that Arg12 was closer to the polar headgroups of

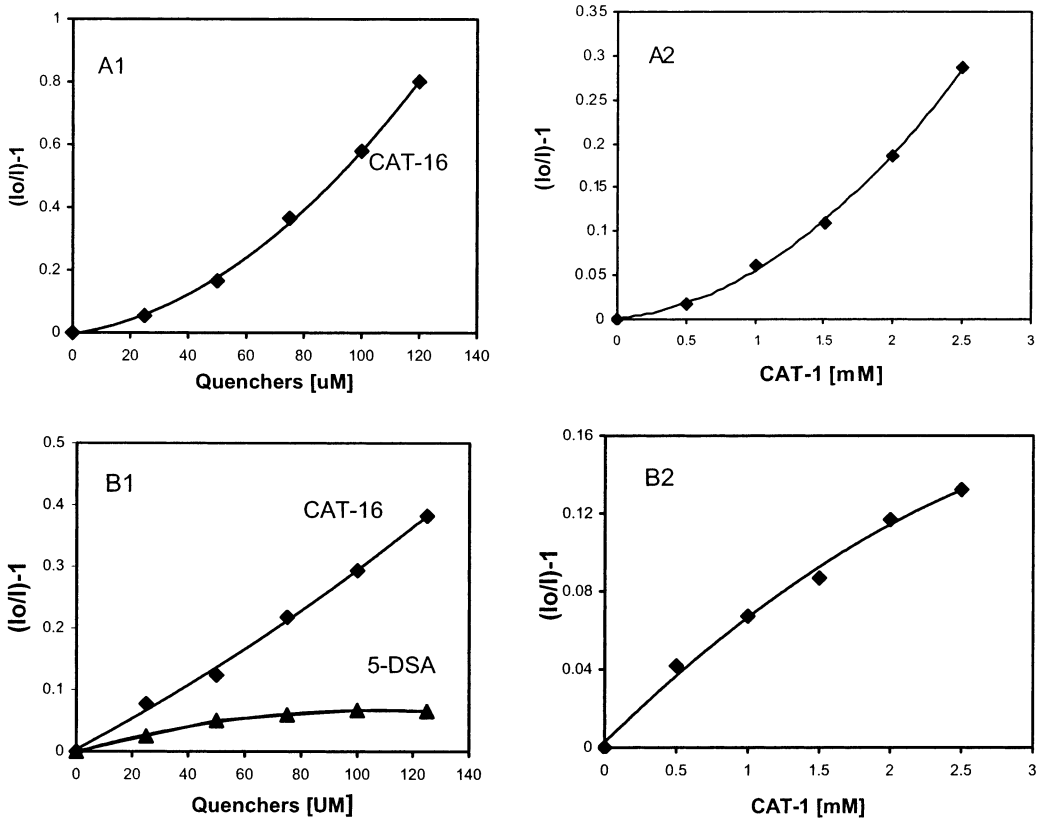

FIGURE 2: Fluorescence quenching of group II peptides. The peptides incorporated into liposomes were suspended in 2 mL of reaction buffer containing 40 μg/mL of the peptides. The reaction was performed at 37 °C. After 4 min of equilibration time, the fluorescence intensity was recorded as described in the Materials and Methods section. The plot was calculated using eq 1. Each point on the plot is the average of three or more experiments.

phospholipids, that is, to the surface of PB, than Gln19. At present, we do not have an explanation for this fact. It may be related to a peculiar bending of the side chain, to specificity of peptide−lipid interactions that distort the ordering of PB, or to something else. The three C-terminal residues, Pro23, Lys24, and Gly25, are located at the surface of PB, just like the N-terminal residues from Phe1 to Pro6. The full profile of the topographical organization of SP-B_{1-25} on PB is depicted in Figure 4.

To rationalize the three-dimensional structure of lipid-associated SP-B_{1-25} in view of the new data, we carried out molecular modeling of the peptide. The primary goal of modeling was to evaluate the measured data with respect to stereochemical considerations imposed by the laws of peptide chemistry, that is, to suggest a set of backbone dihedral angles that are concordant with the results of our fluorescence-quenching experiments. Perfect agreement between the Edmundson diagram and the cyclic pattern in fluorescence-quenching data leaves little doubt about the backbone conformation of the middle part of the peptide. Therefore, the backbone of residues 11−21 was modeled with a standard right-handed α-helix. Because of the very short size of the remaining C-terminal fragment, we do not expect it to form a sequence-specific stable structural form. The conformation of this fragment in the native SP-B, most likely, is influenced by the adjacent protein environment. A maximally extended conformation of this fragment is reasonably consistent with the fluorescence-quenching data.

Assignment of a conformation to the N-terminal part of the peptide represents the most challenging task. Ambiguity in the N-terminus arises from both the irregular pattern of the measured quenching efficiencies and unknown stereoisomerism of the proline residues. There are three highly conserved proline residues in the N-terminal part of the peptide. They are located at positions 2, 4, and 6. Their specific functional role in SP-B is unknown. Generally, proline residues serve as protein secondary-structure disruptors. Also, they are favorably found in the beginning of α-helices, possibly initiating the helical twist. Thus, the three proline residues in the N-terminal part of SP-B may play an important role in maintaining a specific topographical conformation and enhance the surface-active function. We tested their role in a series of peptides in which proline residues were replaced. A peptide with multiple mutations (P2W·P4A·P6A/G25D) was designed specifically to study the role of all three N-terminal proline residues. To keep only one tryptophan residue in the peptide, Trp9 in the native sequence was replaced by tyrosine. On the basis of the observation that the polar quencher CAT-1 and amphiphilic quencher CAT-16 were the most effective quenchers for a tryptophan substitution at position two in the penta-substituted peptide (data not shown), we conclude that substituting all three proline residues with either tryptophan or alanine did not significantly affect the relative location of the side chain of the second residue on PB. Similar results were obtained with single-proline-substituted peptides P2W/A20D, P4W/I22D, and P6W/K24D. These data suggest that under current experimental conditions the conformation of the N-terminal proline residues did not have a significant impact on the topographical organization of the peptide.

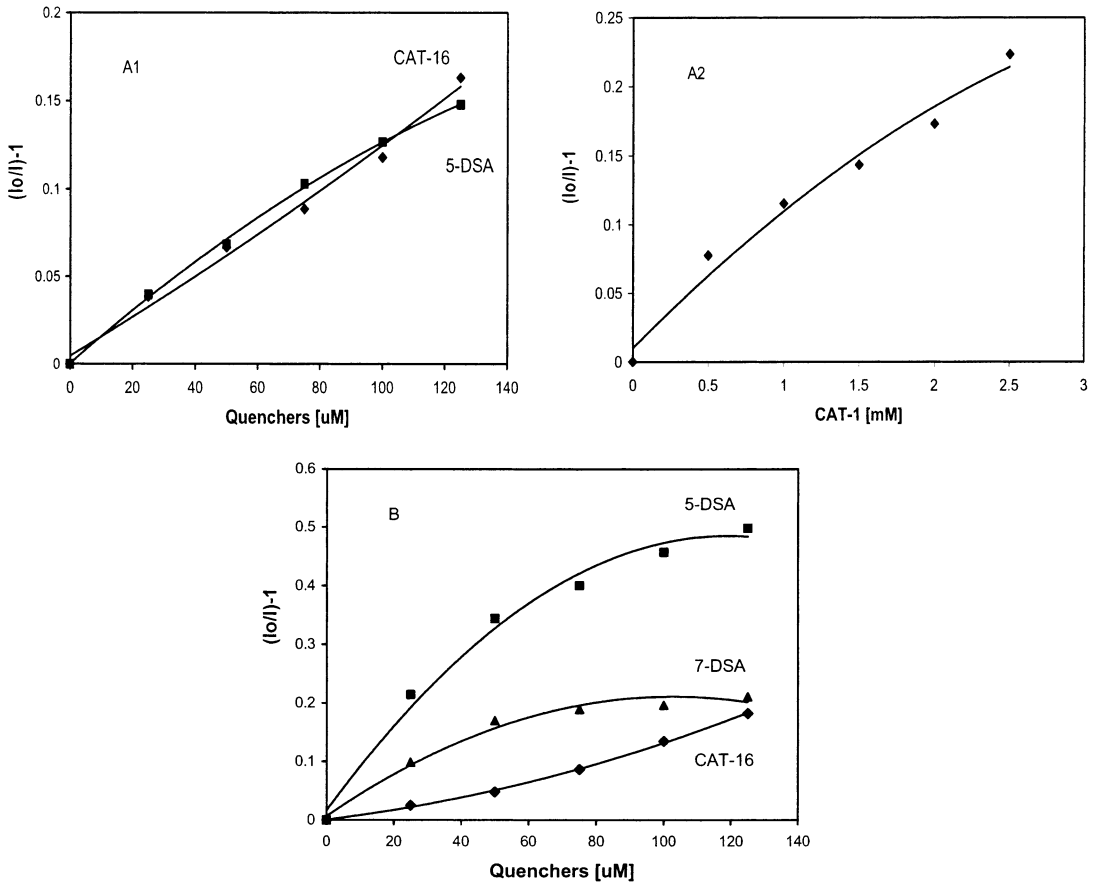

FIGURE 3: Fluorescence quenching of group III peptides. The peptides incorporated into liposomes were suspended in 2 mL of reaction buffer containing 40 μg/mL of the peptides. The reaction was performed at 37 °C. After 4 min of equilibration time, the fluorescence intensity was recorded as described in the Materials and Methods section. The plot was calculated using eq 1. Each point on the plot is the average of three or more experiments.

Because these were substitutions with predominantly trans-peptide residues, all three N-terminal proline residues were modeled in the trans-peptide conformation.

Assignment of the remaining dihedral angles in the N-terminal part of the peptide was started with a test fitting with common canonical conformations. In six independent tests, residues 1−10 were assumed to have one of the standard canonical conformations from the Insight II library as described in the methods section. Next, we calculated the average distance from C_β atoms of each of the ten N-terminal residues either to the hypothetical surface plane or, when appropriate, to a lipid-embedded plane parallel to the surface. The latter plane was placed at 2 Å below the surface. This location is expected to appropriately mimic the natural distance from the 5-DSA probe to a fluorophore, if the fluorophore were located at C_β atoms. The calculated average distances for each of the six tested conformations are listed in Table 4. All of them were unreasonably high. Therefore, the final assignment of the backbone conformation was done manually starting from an extended conformation, which appears to better satisfy the experimental constraints.

The proposed molecular model of SP-B_{1-25} is given in Figure 5. Essentially, it represents a computerized three-dimensional reconstruction of the experimental two-dimensional diagram shown in Figure 4. The Ramachandran plot of the peptide is given in the insert. It shows a concentration of residues in the region of the right α-helix, which corresponds to the middle part of the peptide, and a broad spread of residues in the region of extended conformations. Only Leu10, an interfacial residue between the segments of α-helical and extended conformations, occupies a less common area on the Ramachandran plot in the belt of left-handed helices. The unusual conformation of this residue appears to be essential in linking the two structural regions; otherwise, an appropriate depth for Tyr7, Cys8, and Trp9 in the lipid cannot be achieved. We also observed noticeable noncanonical distortions in the C-terminal part of the helix. Two backbone angles, ψ_{20} and ϕ_{21}, deviate by about 90° from the numbers that are typical for α-helices (Figure 5). These distortions appear to promote the appropriate positioning with respect to PB of other C-terminal residues. However, interestingly, they do not cause a significant impact on the helical pattern of hydrogen bonds. Despite the angular distortions, both Ala20 and Met21 retain an almost perfect hydrogen-bonding network of the helix A, and a helical twist of the ribbon in the pitch that corresponds to these two residues (Figure 5, the last pitch in the bottom panel) visually is almost indistinguishable from the rest of the helix. In-depth computerized refinement of the atomic structure of SP-B_{1-25} based on the available fluorescence-quenching restraints will be presented elsewhere.

The topographic profile of the homodimeric form of SP-B_{1-25} in PB was tested to find out whether there is a change in the topography of the peptide after formation of the intramolecular disulfide bridge. All seven cysteine residues are highly conserved in SP-B. Among them, Cys11, Cys35,

Table 3: Locations of SP-B_{1-25} Residues on PB as Deduced by Fluorescence-Quenching Experiments Using the Synthesized Peptides

tested residues	peptides[a]	order of efficiency of lipid quenchers	CAT-1[b]	predicted locations[c]	predicted conformation[d]
F1	F1W/Q19D	CAT-16	++	S	E
P2	P2W/A20D	CAT-16	++	S	E
I3	I3W/M21D	CAT-16	++	S	E
P4	P4W/I22D	CAT-16	++	S	E
L5	L5W/*P*23D	CAT-16	++	S	E
P6	P6W/K24D	CAT-16	++	S	E
P6	P6D, P6W/K24D	CAT-16	++	S	E
Y7	Y7D	5-DSA > CAT-16		L	
C8	C8D	CAT-16 = 5-DSA	++	L	
W9	W9D	5-DSA > CAT-16		L	
L10	L10D	CAT-16 > 5-DSA	+	S	H
C11	C11D	5-DSA > CAT-16 = 7-DSA		L	H
R12	R12D	CAT-16 > 5-DSA	++	W	H
A13	A13D	CAT-16	++	W	H
L14	L14D	5-DSA ≥ CAT-16	++	L	H
I15	I15D	5-DSA > 7-DSA		L	H
K16	K16D	none	+	W	H
R17	R17D	CAT-16 > 5-DSA	+	S	H
I18	I18D	5-DSA > 7-DSA		L	H
Q19	F1W/Q19D	none	+	W	H
A20	P2W/A20D	none	+	W	H
M21	I3W/M21D	5-DSA ≥ CAT-16 > 7-DSA	+	L	H
I22	P4W/I22D	5-DSA > CAT-16 > 7-DSA		L	H
*P*23	L5W/*P*23D	CAT-16 > 5-DSA = 7-DSA	+	S	
K24	P6W/K24D	CAT-16 > 5-DSA	+	S	E
G25	P2W·P4A·P6A/G25D	CAT-16 > 5-DSA	+	S	E

[a] In multiple-substituted peptides, the peptide was not labeled with NCD-4 when tryptophan was used as a source of autofluorescence. [b] The + marker under the hydrophilic quencher CAT−1 represents a degree of quenching efficiency by CAT-1. More markers indicate a stronger effect. [c] S stands for the surface of PB, L stands for lipid, and W stands for water environment. [d] H stands for the α-helical conformation, and E stands for extended conformation.

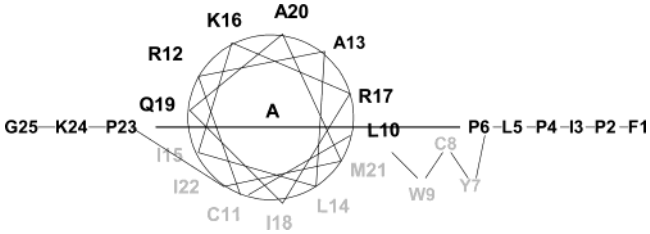

FIGURE 4: Two-dimensional diagram showing the relative locations of residues with respect to PB. The Edmundson helical wheel denotes the helical portion of the peptide. The diagram shows that residues Leu10−Ile22 form an amphipathic helix that is half-embedded in PB. One side of the helix consisting of residues Arg12, Ala13, Lys16, Arg17, Gln19, and Ala20 oversees the polar environment, while the other consisting of residues Ile15, Ile22, Cys11, Ile18, Leu14, and Met21 is embedded in PB (gray-colored). The N-terminal Phe1−Pro6 and the C-terminal Pro23−Gly25 are located at the lipid−water interface. Irregularly structured Tyr7−Trp9 are embedded in PB. The horizontal line represents the surface of PB.

Table 4: Average Per Residue Distance from C_β Atoms of Residues 1−10 to a Point of Appropriate PB-Associated Spatial Constraint Derived from the Fluorescence-Quenching Experiments

conformation	distance (Å)
3_{10}-helix	3.07
β-strand	2.76
π-helix	2.75
α-helix, left	2.49
α-helix, right	2.31
extended	2.28
manual	0.96

Cys46, and Cys71 are predicted to be located at the hydrophobic sides of helices A, B, C, and D of SP-B, respectively (*24*). Cys11 of helix A and Cys71 of helix D form an intramolecular disulfide bond. The results of quenching experiments for the C11D peptide indicate that Cys11 is located at the bottom of the hydrophobic side of amphipathic helix A (Figure 4) facing the lipids. To form a disulfide bond with Cys71 of the neighboring amphipathic helix D, Cys11 may have to rotate at an angle to face the partner. Therefore, a dimer of the C8D peptide (dC8D) was used in quenching experiments to investigate the topographic changes associated with formation of the intramolecular disulfide bond. Because in this peptide Cys8 was replaced by aspartate, Cys11 becomes the only cysteine residue capable of dimerization. Two fluorescent groups, NCD-4-labeled Asp8 (in the native sequence Cys8) and Trp9, were utilized to monitor sulfhydryl-dependent conformational and topographic changes. The effective quenching order for Asp8 in C8D was CAT-16 = 5-DSA (Figure 3A) suggesting that Asp8 was located close to the surface of PB.

However, the effective quenching order for the homodimer dC8D was CAT-16 > 5-DSA (Figure 6A), thus suggesting that in the dimeric form of the peptide Asp8 is reoriented and directed more toward the aqueous environment. Similar results were obtained using the fluorescence quenching of Trp9. The order of effective quenching for Trp9 was 5-DSA ≫ 7-DSA in the C8D monomer (Figure 6B). However, in dC8D, it has changed to CAT-16 > 5-DSA (Figure 6C). This suggests that in dC8D Trp9 also changed its topographic position compared to the monomer and moved toward the surface of PB.

These results imply that upon the disulfide bond formation the helix A turns at an angle to the PB surface as compared to the monomer form of SP-B_{1-25}. Therefore, Cys11 rotates and moves from a deeper to shallower location in the PB,

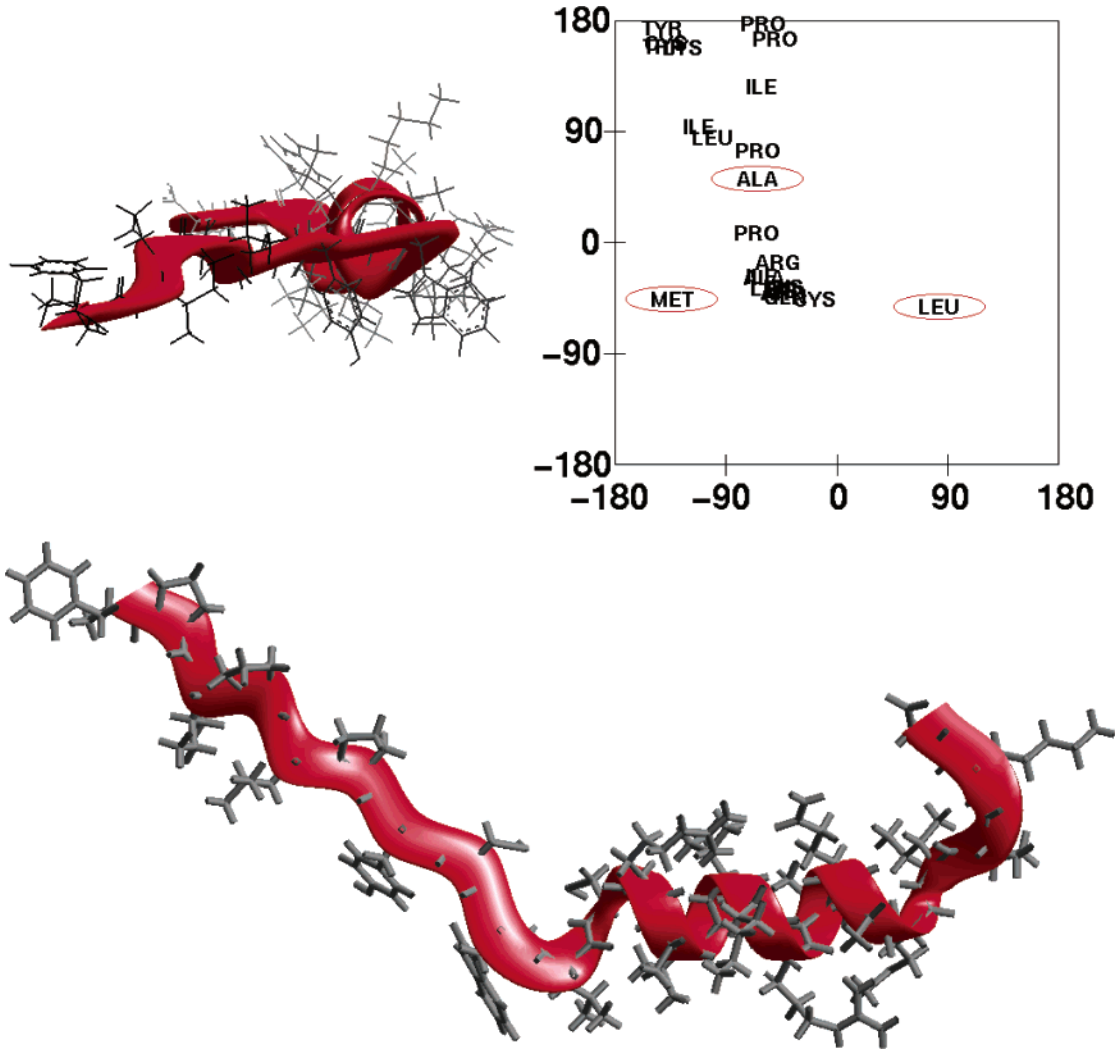

FIGURE 5: Molecular model of SP-B_{1-25} that satisfies the fluorescence-quenching data. The bottom panel represents SP-B_{1-25} viewed from the solvent side of the peptide−PB complex. The N-terminus is to the left. The side view of the molecule is given in the upper left panel. The N-terminus faces the reader; PB is assumed to be underneath the molecule. Details of the backbone conformation are summarized in the Ramachandran plot in the upper left insert. Leu10, Ala20, and Met21 discussed in the text are circled.

which facilitates the sulfhydryl-dependent association with the neighboring helix (Figure 7A).

DISCUSSION

SP-B_{1-25} is a functionally important N-terminal fragment of the lung pulmonary surfactant protein B, which by itself can mimic many physiological effects of the whole protein. A truncated peptide lacking this fragment shows inferior properties (*39*). Structural characterization of SP-B_{1-25} and its topographical organization in phospholipid membranes is essential for understanding the mechanism of action of SP-B. We used a position-wise fluorescent group labeling technique to test the depth of each residue on PB. Fluorescence-quenching experiments were carried out either on tryptophan- or NCD-4/aspartate-substituted peptides reconstituted in PB. Using these experiments, we determined the location of each of the 25 residues with respect to the surface of PB.

The results suggest that SP-B_{1-25} is located at the surface of PB without forming a transmembrane domain or even significantly penetrating inside PB. The side chains of all residues are located in the interfacial region between the polar phase and lipids up to a depth of carbon-5 of the fatty acid chains. This conclusion is based on the observation that the polar quencher CAT-1, amphiphilic quencher CAT-16, and hydrophobic quencher 5-DSA were the most effective quenchers for all of the substituted peptides. Interactions of the fluorescent probes with deeper hydrophobic quenchers, for example, 7-DSA and 12-DSA, were much weaker, or there was no detectable effect at all. These data imply that SP-B_{1-25} essentially rests on the surface of the lipid−water interface. This is consistent with many previous reports suggesting a shallow profile of SP-B_{1-25} on the lipids (*32*, *33*, *48*, *53*) and disagrees with the literature proposing a deeper location for the peptide (*44*).

Our data show that the first six residues of the peptide (Phe1−Pro6) are confined to a thin interfacial layer between the lipids and aqueous phase of the system. The most likely conformation of these residues belongs to a structural class that is distinct from the α-helix. It has been previously suggested that these residues may be in a β-sheet conformation (*33*, *34*). Our results indicate that these residues, strictly speaking, do not form a classical Pauling−Corey β-strand. However, they do map close to this region on the Ramachandran plot and thus may be considered as a more general class of extended conformations that includes the β-structure

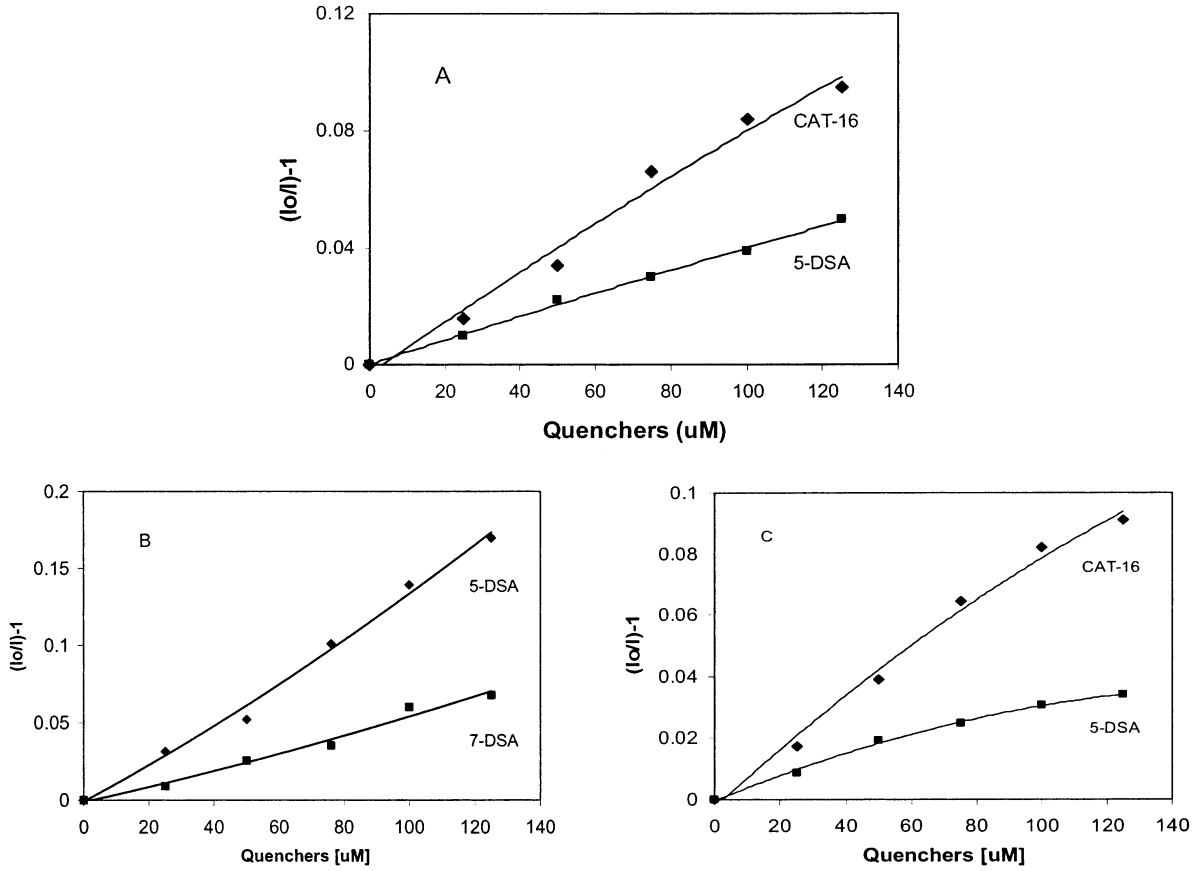

FIGURE 6: Fluorescence-quenching efficiency for Asp8 and Trp9 in monomer (C8D) and dimer (dC8D) peptides. In these peptides, Cys8 was substituted with NCD-4-labeled aspartate. Cys11 was the only residue that was able to participate in the disulfide bond formation. Panel A shows fluorescence quenching for Asp8 in the NCD-4-labeled dC8D dimer. Panel B shows fluorescence quenching for Trp9 in the C8D monomer. Panel C shows fluorescence quenching for Trp9 in the dC8D dimer. The peptides incorporated into liposomes were suspended in 2 mL of reaction buffer containing 40 μg/mL of the peptides. The reaction was performed at 37 °C. After 4 min of equilibration time, the fluorescence intensity was recorded as described in the Materials and Methods section. The plot was calculated using eq 1. Each point on the plot is the average of three or more experiments.

as a subclass. In a computerized test of six standard regular conformations, we observed that an extended conformation better matches the experimental endpoints (Table 4). Minor manual adjustment of the extended conformation resulted in a drastic improvement of the fit, which we were not able to achieve using helical conformations. The N-terminal sequence contains a pattern of three equally spaced proline residues, which may be central to the function of the fragment. Because of the lack of amide hydrogen atom and restrictions imposed by the pyrrolidine ring, proline residues usually do not promote regular secondary structures (except for special cases of poly(Pro) helices). Therefore, it is hard to expect a classical type of β-conformation in the N-terminal part of SP-B.

Implications of proline substitutions to topographical mapping of SP-B_{1-25} on PB were studied using several appropriately selected synthetic peptides. They are P6D, P2W/A20D, P4W/I22D, P6W/K24D, and P2W·P4A·P6A/G25D. The latter was specifically designed to investigate the conformational importance of the simultaneous presence of all three proline residues. In this peptide, a tryptophan probe was placed at the second position, thus creating a unique autofluorescent group in the NCD-4 unlabeled peptide. Quenching experiments with multiple-mutation peptides, including P2W·P4A·P6A/G25D, revealed that the location of the first six N-terminal residues on the surface

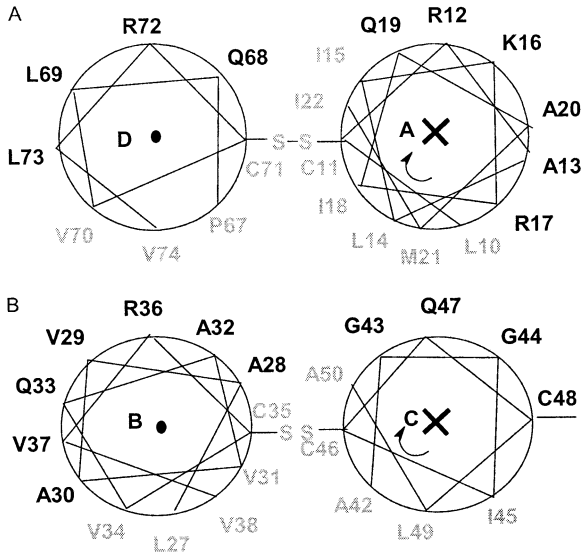

FIGURE 7: Edmundson helical wheel diagrams representing a side view of proposed relative orientations of helices A and D (A) and B and C (B) after the intramolecular disulfide bond formation. The helix A rotates at an angle of about 90° compared to the reduced form (Figure 4). A similar process may also take place with helices B and C. The (X) mark in the helix center denotes that the C-terminus faces the reader, while the (●) mark denotes that the N-terminus facing the reader. Nonpolar residues are represented by the gray color.

of PB was not disturbed by any of these substitutions. We did not observe any significant variation in the depth of N-terminal residues between peptides that did not carry substitutions in the N-terminal proline residues, for example, F1W/Q16D, I3W/M21D, and L5W/P23D (Table 2), and those with substitutions. Therefore, we conclude that interactions of the N-terminal region with phospholipid headgroups do not rely on the proline residues. Unlike in some short peptides (*54*), it is likely that all N-terminal proline residues in SP-B_{1-25} adopt a predominately trans conformation. The structural and functional role of these conserved proline residues remains to be elucidated. Possibly, they serve as signals preventing structural ordering of the N-terminus in either an elongated helix A or a specific nonhelical structural motif, presumably the β-structure (*33*, *34*). Another possibility would be to assume that in a different environment they may be responsible for a cis−trans isomerization, which may result in a yet undisclosed structural shape of the N-terminus, for example, a hypothetical "biochemical Velcro" (*55*).

The role of N-terminal proline residues may be closely related to conformation of the next few residues before the α-helix. They are Tyr7, Cys8, and Trp9. If these residues adopt an α-helical conformation, that is, belong to the helix A, then according to the Edmundson diagram of Figure 4, the side chain of Trp9 shall be exposed to the solvent and Cys8 shall be located in proximity to the phospholipid headgroups. However, according to our measurements, each of the NCD-4-labeled Y7D, C8D, and W9D peptides strongly interacts with the nonpolar quencher 5-DSA. Therefore, all of these three residues appear to be embedded in PB, which would lead to a conclusion that Cys8 and Trp9 may not be involved in the α-helix, and thus, the helical segment on SP-B_{1-25} may not start before Lys10.

Concerning peptide folding, one may doubt that a negatively charged aspartate, albeit NCD-4-labeled, is a good substituent for hydrophobic side chains of key helix-initiating residues. To confirm that indeed Trp9 is not involved in the helix, its location was additionally investigated using tryptophan autofluorescence. The experiments were performed with NCD-4 unlabeled peptides Y7D, C8D, and L10D, in which Trp9 was the only source of autofluorescence. In these experiments, 5-DSA was the most effective quencher for each of the three peptides (data not shown). These experiments additionally confirm the conclusion that indeed Trp9 is embedded in PB. In a recent study, the distance between the center of PB and Trp9 was estimated to be 10−13 Å (*48*), which is in accord with our current result. However, earlier studies have been suggesting a shallower location of the residue (*33*, *56*).

It has been proposed that the topographical and structural organization of SP-B may depend on experimental conditions such as the liposome content of lipid components, lipid/protein ratio, and conditions of peptide incorporation into the liposomes (*48*, *50*, *57*, *58*). Also, it has been reported that the location of Trp9 on PB is sensitive to microenvironmental conditions (*34*, *50*). This may explain the observed variability in the depth of Trp9 on PB, along with the differences in estimated length of the helix A. In a recent NMR study of SP-B_{11-25} in a structure-promoting environment, it was shown that the helical conformation extends from Leu14 to Met21 only (*39*). This further confirms the possibility that the length of helix A may vary depending on experimental conditions.

Our data suggest that the helix A in a PB-bound form of SP-B_{1-25} can stretch from Leu10 to Ile22. Because the fluorescence quenching of the NCD-4 chromophore by a polar quencher CAT-1 could not be detected either in C11D or in P4W/I22D peptides (in which the locations of chromophore approximately designate the ends of the α-helix), we conclude that the side chains of both Cys11 and Ile22 are embedded inside PB, and thus the α-helix in the SP-B_{1-25} peptide is attached to PB essentially parallel to the surface of the water−lipid interface. This is a somewhat unexpected result because previous studies, which relied on either physical (*33*, *39*) or computational (*44*) methods, postulated a tilted model of the peptide on the surface. At present, we do not have an explanation for this discrepancy. It may be related to variations in experimental conditions, microenvironment, or the method of peptide reconstitution in liposomes. A recent report shows that the depth of SP-B in PB may indeed depend on the method of reconstitution (*58*). In that study, the authors observed that SP-B reconstituted from lipid/protein mixtures in organic solvents was inserted more deeply in PB than proteins reconstituted by the addition to already preformed phospholipid vesicles. We prepared the liposomes by adding the peptides to preformed vesicles; therefore, the topographic model described in this paper may represent a new shallow mode of SP-B_{1-25} on PB.

It has been reported that sulfhydryl-dependent dimers of SP-B_{1-25} are more surface-active compared to the molecules without disulfide bonds (*27*); however, the molecular mechanism of observed differences remains unknown. Our data suggest that in the peptide without disulfide bonds Cys8 and Trp9 are embedded in PB, Cys8 being superficial to Trp9. In the dimer, both residues rotate by an angle, bringing Cys8 into a position outside of PB while Trp9 moves closer to the surface. This configurational rearrangement implies that the disulfide bond formation induces a change in the protein−lipid interactions such that the helices of the two peptides face each other with amphipathic sides of the helices, thereby forming a hydrophobic domain. Interestingly, early immunologic studies indicated that conformation of the N-terminal part of SP-B is sensitive to disulfide bond formation (*59*). Therefore, we expect that the consequences of the sulfhydryl-dependent rotation of the helix A discovered in this work also hold for the full-size SP-B, that is, that interactions between the helix A and helix D, and between their jointly formed hydrophobic domain and phospholipids, may be similar to those described in the present study. Also, we project that similar principles apply to helices B and C, which taken together may form another hydrophobic domain complementary to helices A and B. In polar environments, the two domains may interact forming, for instance, a saposin-like fold as postulated by a recent homology model (*20*). In nonpolar environments, the self-packed structural assembly of the protein may spontaneously unfold promoting spreading of lipids from the collapse phase to the air/liquid interface (*27*, *60*−*63*). The possibility of such conformational restructuring is evident from conformational transformations of SP-B in various aqueous−organic solvents (*50*), although mechanically this process requires coherent straightening of two "molecular hinges" between the helices A and B and C

and D. In a close-ring topology of the backbone with coils (confined by disulfide bridges), this is a nontrivial motion. However, if the proposed type of conformational rearrangement indeed takes place, then SP-B may gain the ability to reversibly carry nonpolar materials in and out of the polar phase. Dimerization of the molecule will enhance both effects. Formation of sulfhydryl-dependent dimers has been shown to be beneficial for phospholipid trafficking in the lung (*64*).

It has been recently shown that amphiphilic block copolymers can stabilize PB interactions in a bicontinuous phase because of increased rigidity of surfactant (*65*). In the lung, quasi-regular surfactant formations, for example, the lamellar bodies, are secreted into the alveolar fluids by exocytosis of epithelial type II pneumocytes. The lamellar bodies form a tubular network (tubular myelin). The tubular myelin absorbs at the air/liquid interface forming a phospholipid-rich film. During the ventilation cycle, this complex structural system spreads and recovers the lipid material of the interfacial film. It has been demonstrated that amphiphilic SP-B acts as a helper in this process (*15*, *27*). Superproduction of lung pulmonary surfactant observed in certain clinical situations, for instance, in silicosis, may disrupt this process by shifting the water/lipid ratio in the bicontinuous phase of the lung toward a lamellar−sponge transition. Thus, the level of expression and concentration of SP-B in the surfactant−water mixture would play an important role in the lung (*14*, *15*), guiding the exchange between the surface, lamellar, and sponge phases (*66*). We hypothesize that the folded and open (amphiphilic) forms of SP-B may reversibly interchange in response to variations in the alveolar surface tension, thus promoting phospholipid traffic to and from the interfacial lining film. The new binding mode of SP-B_{1-25} in PB described in this work gives new insights into the conformational and topographical transitions that the protein might undergo. This structural lability of the protein, perhaps, is the most important physiological property of SP-B.

ACKNOWLEDGMENT

Technical assistance of Terence G. Meighan, Mark Barger, and Donna Pack is greatly appreciated.

REFERENCES

1. Clements, J. A. (1977) *Am. Rev. Respir. Dis. 115*, 67.
2. Piknova, B., Schram, V., and Hall, S. B. (2002) *Curr. Opin. Struct. Biol. 12*, 487.
3. Wang, Z. D., Hall, S. B., and Notter, R. H. (1996) *J. Lipid Res. 37*, 790.
4. Oosterlaken-Dijksterhuis, M. A., Haagsman, H. P., van Golde, L. M., and Demel, R. A. (1991) *Biochemistry 30*, 8276.
5. Johansson, J., and Curstedt, T. (1997) *Eur. J. Biochem. 244*, 675.
6. Notter, R. H., Wang, Z., Egan, E. A., and Holm B. A. (2002) *Chem. Phys. Lipids 114*, 21.
7. Curstedt, T., Hornvall, H., Robertson, B., Bergman, T., and Berggren, P. (1997) *Eur. J. Biochem. 168*, 255.
8. Schram, V., and Hall, S. B. (2001) *Biophys. J. 81*, 1536.
9. Taneva, S. G., and Keough, K. M. W. (1994) *Biochemistry 33*, 14660.
10. Diemel, R. V., Snel, M. M. E., Waring, A. J., Walther, F. J., van Golde, L. M. G., Putz, G., Haagsman, H. P., and Batenburg, J. J. (2002) *J. Biol. Chem. 277*, 21179.
11. Poulain, F. R., Allen, L., Williams, M. C., Hamilton, R. L., and Hawgood, S. (1992) *Am. J. Physiol. 262*, L730.
12. Kaser, M. R., and Skoutreis, G. G. (1997) *Peptides 18*, 1441.
13. Baatz, J. E., Zou, Y., and Flume, P. A. (1999) *Am. J. Respir. Crit. Care. 159* (Suppl. S), A895.
14. Clark, J. C., Wert, S. E., Bachurski, C. J., Stahlman, M. T., Stripp, B. R., Weaver, T. E., and Whitsett, J. A. (1995) *Proc. Natl. Acad. Sci. U. S. A. 92*, 7794.
15. Stahlman, M. T., Gray, M. P., Falconieri, M. W., Whitsett, J. A., and Weaver, T. E. (2000) *Lab. Invest. 80*, 395.
16. Johansson, J., Curstedt, T., and Jornvall, H. (1991) *Biochemistry 30*, 6917.
17. Andersson, M., Curstedt, T., Jornvall, H., and Johansson, J. (1995) *FEBS Lett. 362*, 328.
18. Weaver, T., and Conkright, J. (2001) *Annu. Rev. Physiol. 63*, 555.
19. Patthy, L. (1991) *J. Biol. Chem. 266*, 6035.
20. Zaltash, S., Palmblad, M., Curstedt, T., Johansson, J., and Persson, B. (2000) *Biochim. Biophys. Acta 1466*, 179.
21. Cochrane, C. G., and Revak, S. D. (1991) *Science 254*, 566.
22. Longo, M. L., Bisagno, A. M., Zasadzinski, J. A., Bruni, R., and Waring, A. J. (1993) *Science 261*, 453.
23. Flanders, B. N., Vickery, S. A., and Dunn, R. C. (2001) *J. Microsc. (Oxford) 202* (Part 2), 379.
24. Flanders, B. N., Vickery, S. A., and Dunn, R. C. (2002) *J. Phys. Chem. B 106*, 3530.
25. Lee, K. Y. C., Lipp, M. M., Zasadzinski, J. A., and Waring, A. J. (1997) *Colloids Surf., A 128*, 225.
26. Bringezu, F., Ding, J. Q., Brezesinski, G., Waring, A. J., and Zasadzinski, J. A. (2002) *Langmuir 18*, 2319.
27. Veldhuizen, E. J. A., Waring, A. J., Walther, F. J., Batenburg, J. J., van Golde, L. M. G., and Haagsman, H. P. (2000) *Biophys. J. 79*, 377.
28. Gupta, M., Hernandez-Juviel, J. M., Waring, A. J., and Walther, F. J. (2001) *Thorax 56*, 871.
29. Gupta, M., Hernandez-Juviel, J. M., Waring, A. J., Bruni, R., and Walther, F. J. (2000) *Eur. Respir. J. 16*, 1129.
30. Vandenbussche, G., Clercx, A., Clercx, M., Curstedt, T., Johansson, J., Jornvall, H., and Ruysschaert, J. M. (1992) *Biochemistry 31*, 9169.
31. Pastrana-Rios, B., Taneva, S., Keough, K. M. W., Mautone, A. J., and Mendelsohn, R. (1995) *Biophys. J. 69*, 2531.
32. Dieudonne, D., Mendelsohn, R., Farid, R. S., and Flach, C. R. (2001) *Biochim. Biophys. Acta 1511*, 99.
33. Gordon, L. M., Horvath, S., Longo, M. L., Zasadziniski, J. A., Taeusch, H., Faull, K., Leung, C., Waring, A. J. (1996) *Protein Sci. 5*, 1662.
34. Gordon, L. M., Lee, K. Y. C., Lipp, M. M., Zasadzinski, J. A., Walther, F. J., Sherman, M. A., and Waring, A. J. (2000) *J. Pept. Res. 55*, 330.
35. Kang, J. H., Lee, M. K., Kim, K. L., and Hahm, K. S. (1996) *Biochem. Mol. Biol. Int. 40*, 617.
36. Pérez-Gil, J., Cruz, A., and Casals, C. (1993) *Biochim. Biophys. Acta 1168*, 261.
37. Bruni, R., Taeusch, H. W., and Waring, A. J. (1991) *Proc. Natl. Acad. Sci. U.S.A. 88*, 7451.
38. Morrow, M. R., Taneva, S., Dico, A. S., Hancock, J., and Keough, K. M. W. (1997) *Biochem. Soc. 25*, 1103.
39. Kurutz, J. W., and Lee, K. Y. C. (2002) *Biochemistry 41*, 9627.
40. Dico, A. S., Hancock, J., Morrow, M. R., Stewart, J., Harris, S., and Keough, K. M. W. (1997) *Biochemistry 36*, 4172.
41. Dico, A. S., Hancock, J., Morrow, M. R., Stewart, J., and Keough, K. M. W. (1997) *Biophys. J. 72* (Part 2), WP366.
42. Vincent, J. S., Revak, S. D., Cochrane, C. G., and Levin, I. W. (1991) *Biochemistry 30*, 8395.
43. Baatz, J. E., Elledge, B., and Whitsett, J. A. (1990) *Biochemistry 29*, 6714.
44. Kaznessis, Y., Kim, S., and Larson, R. (2002) *J. Mol. Biol. 322*, 569.
45. London, E. M., and Feifensen, G. W. (1981) *Biochemistry 20*, 1932.
46. Blatt, E., Chatelier, R. C., and Sanyer, R.C. (1984) *Photochem. Photobiol. 39*, 477.
47. Wang, Y. D., and Beattie, D. S. (1993) *Biochemistry 32*, 9586.
48. Cruz, A., Casals, C., Plasencia, I., Marsh, D., and Pérez-Gil, J. (1998) *Biochemistry 37*, 9488.
49. Lacowicz, J. R. (1983) *Principles of Fluorescence Spectroscopy*, p 260, Plenum Press, New York.
50. Cruz, A., Casals, C., Pérez-Gil, J. (1995) *Biochim. Biophys. Acta 1225*, 68.
51. Brooks, B. R., Bruccoleri, R. E., Olafson, B. D., States, D. J., Swaminathan, S., Karplus, M. (1983) *J. Comput. Chem. 4*, 187.
52. MacKerell, A. D., Jr., Bashford, D., Bellott, M., Dunbrack, R. L., Jr., Evanseck, J. D., Field, M. J., Fischer, S., Gao, J., Guo, H., Ha, S., Joseph-McCarthy, D., Kuchnir, L., Kuczera, K., Lau, F.

T. K., Mattos, C., Michnick, S., Ngo, T., Nguyen, D. T., Prodhom, B., Reiher, W. E., III, Roux, B., Schlenkrich, M., Smith, J. C., Stote, R., Straub, J., Watanabe, M., Wiorkiewicz-Kuczera, J., Yin, D., and Karplus, M. (1998) *J. Phys. Chem. B 102*, 3586.

53. Lee, K. Y. C., Majewski, J., Kuhl, T., Howes, P. B., Kjaer, K., Lipp, M. M., Waring, A. J., Zasadzinski, J. A., and Smith, G. S. (2000) in *Applications of Synchrotron Radiation Techniques to Materials Science*, (Stock, S. R., Mini, S. M., Perry, D. L., Eds.) Materials Research Society Symposium Proceedings, Vol. 590, p 177, Materials Research Society, Warrendale, PA.
54. Yao, J., Feher, V. A., Espejo, B. F., Reymond, M. T., Wright, P. E., and Dyson, H. J. (1994) *J. Mol. Biol. 243*, 736.
55. Pérez-Gil, J., and Keough, K. M. W. (1991) *Biochem. Int. 25*, 715.
56. Griffith, O. H., Dehlinger, P. J., and Van, S. P. (1974) *J. Membr. Biol. 15*, 159.
57. Shanmukh, S., Howell, P., Baatz, J. E., and Dluhy, R. A. (2002) *Biophys. J. 83*, 2126.
58. Cruz, A., Casals, C., Keough, K. M. W., and Pérez-Gil, J. (1997) *Biochem. J. 327* (Part 1), 133.
59. Fan, B. R., Bruni, R., Taeusch, H. W., Findlay, R., and Waring, A. J. (1991) *FEBS Lett. 282*, 220.
60. Lipp, M. M., Lee, K. Y. C., Takamoto, D. Y., Zasadzinski, J. A., and Waring, A. J. (1998) *Phys. Rev. Lett. 81*, 1650.
61. Ding, J., Takamoto, D. Y., van Nahamen, A., Lipp, M. M., Lee, K. Y. C., Waring, A. J., and Zasadzinski, J. A. (2001) *Biophys. J. 80*, 2262.
62. Takamoto, D. Y., Lipp, M. M., von Nahmen, A., Lee, K. Y. C., Waring, A. J., and Zasadzinski, J. A. (2001) *Biophys. J. 81*, 153.
63. Lipp, M. M., Lee, K. Y. C., Zasadzinski, J. A., and Waring, A. J. (1996) *Science 273*, 1196.
64. Beck, D. C., Na, C. L., Whitsett, J. A., and Weaver, T. E. (2000) *J. Biol. Chem. 275*, 3371.
65. Mihailescu, M., Monkenbusch, M., Endo, H., Allgaier, J., Gompper, G., Stellbrink, J., Richter, D., Jakobs, B., Sottmann, T., and Farago, B. (2001) *J. Chem. Phys. 115*, 9563.
66. Boghosian, B. M. (1999) *Future Gener. Comput. Syst. 16*, 171.

BI027344H